

# Measuring rotational diffusion of macromolecules by fluorescence correlation spectroscopy

Anastasia Loman,<sup>a</sup> Ingo Gregor,<sup>a</sup> Christina Stutz,<sup>b</sup> Markus Mund<sup>b</sup> and Jörg Enderlein<sup>\*a</sup>

Received 16th June 2009, Accepted 3rd November 2009

First published as an Advance Article on the web 4th December 2009

DOI: 10.1039/b9pp00029a

We describe a novel method to measure rotational diffusion of large biomolecules in solution based on fluorescence correlation on the nanosecond time scale. In contrast to conventional fluorescence anisotropy measurements, a correlation-based method will also work if the rotational diffusion time is much longer than the fluorescence decay time. Thus, the method is suited to study the rotational diffusion of macromolecules having rotational diffusion times of dozens to hundreds of nanoseconds, which is considerably larger than the fluorescence lifetime of most commercially available dyes or auto-fluorescent proteins. A pulsed interleaved excitation scheme with crossed excitation polarization maximizes the time-dependent amplitude of the measured correlation curve as caused by rotational diffusion. Using the determined rotational diffusion coefficient, precise values of the hydrodynamic radius can be obtained. The method is exemplified on sizing a set of common globular proteins.

## Introduction

Thermally induced translational and rotational diffusion are fundamental dynamic processes of molecules within a solution. The Stokes–Einstein relation,

$$D_{\text{trans}} = \frac{k_{\text{B}}T}{6\pi\eta R_{\text{trans}}} \quad (1)$$

connects the translational diffusion coefficient  $D_{\text{trans}}$  of a molecule with its hydrodynamic radius  $R_{\text{trans}}$ ,<sup>1</sup> where, in the above equation,  $k_{\text{B}}$  is Boltzmann's constant,  $T$  the absolute temperature, and  $\eta$  the solvent's viscosity. Dual-focus fluorescence correlation spectroscopy (2fFCS)<sup>2</sup> allows the measurement of precise absolute values of the translational diffusion coefficient of macromolecules close to the infinite dilution limit

Also the rotational diffusion coefficient  $D_{\text{rot}}$  of a molecule is connected to a value of its hydrodynamic radius  $R_{\text{rot}}$ , via the Stokes–Einstein–Debye equation,<sup>3</sup>

$$D_{\text{rot}} = \frac{k_{\text{B}}T}{8\pi\eta R_{\text{rot}}^3} \quad (2)$$

Rotational diffusion is usually determined by static or dynamic fluorescence anisotropy measurements.<sup>4</sup> This method requires fluorescent labels with a fluorescence lifetime in the order of the rotational diffusion time. However, the rotational diffusion time of macromolecules such as globular proteins is in the order of several dozen nanoseconds, which requires the use of rather uncommon long-lifetime probes. Here, we will use fluorescence correlation measurements in the nanosecond time-range to obtain rotational

diffusion coefficients. Theoretical and experimental studies to determine rotational diffusion coefficients using fluorescence correlation spectroscopy (FCS) have been published before.<sup>5–9</sup> The method has the advantage of being independent of the label's fluorescence lifetime and is also rather independent of the details of excitation and detection polarization. Moreover, one can use the same fluorescent label and same optical set-up for measuring both translational and rotational diffusion and directly compare both values. The conventional approach to measure rotational diffusion using FCS is to excite the sample with a linearly polarized continuous-wave excitation laser, and to monitor the fluorescence through either linear polarizers, or in non-polarized detection mode. Here, we propose a more complex but also more efficient excitation/detection scheme: fluorescence is excited by a train of laser pulses with alternating polarization. Fluorescence detection is done by time-correlated single photon counting in two detection channels with crossed detection polarization. High-speed detection electronics independently times photon detection events in both detection channels with picosecond accuracy. By this we can unequivocally assign each detected photon to its exciting laser pulse (and thus excitation polarization), and calculate the cross correlation between photons from the two detection channels down to picosecond correlation times. The advantages of using such an excitation/detection scheme are two-fold: using a pulsed excitation improves the signal-to-noise statistics due to photon bunching, and one can extract a correlation function that has largest rotational-diffusion related amplitude (see Theory section).

In this paper, we apply the new method to size four different globular proteins; two of them belong to a large family of serum albumins: bovine serum albumin (BSA) and human serum albumin (HSA). BSA is the most studied example of a serum albumin, which has attracted considerable attention over the past decades (see ref. 10 and references therein). The other two proteins studied here are aldolase from rabbit muscles, and hen egg ovalbumin.

<sup>a</sup>III. Physikalisches Institut, Georg-August-Universität, D-37077, Göttingen, Germany. E-mail: enderlein@physik3.gwdg.de; Fax: +49-551-397720; Tel: +49-551-3913833

<sup>b</sup>Eberhard-Karls-Universität, D-72074, Tübingen, Germany

## Theory

### Autocorrelation function (ACF)

On a pico- to nanosecond timescale, the ACF is characterized by fluorescence antibunching and rotational diffusion. Fluorescence antibunching is caused by the fact that a single emitter with a finite lifetime of its excited state can just emit one single photon at a time. It can be used to obtain the average number of emitters within the detection volume.<sup>11–15</sup> Rotational diffusion will be seen in the ACF if one excites/detects fluorescence in a polarization-sensitive manner. Due to the rotation of a molecule between different photon excitation and emission events and thus rotation of the molecule's dipole axis into or out of the polarization plane of the detector, the correlation of the recorded fluorescence signal will show a temporal component that is related to the rotational diffusion of the molecule.<sup>5–9</sup>

Let us consider an experiment where the sample is excited with two consecutive pulses of negligible pulse width. In such a measurement, what is the probability of detecting two photons from one and the same molecule with lag time  $t$  between them? If we assume that the fluorescence decay is mono-exponential with decay time  $\tau$ , and if we take further into account that a molecule can emit, after one excitation pulse, only one photon, this probability will be proportional to

$$\int_{\min(\delta-t, 0)}^{\delta} dt_1 \frac{\kappa_1}{\tau} e^{-t_1/\tau} \frac{\kappa_2}{\tau} e^{-(t_1+t-\delta)/\tau} = \kappa_1 \kappa_2 F_1(t, \tau, \delta) \quad (3)$$

where we have introduced the function

$$F_1(t, \tau, \delta) = \frac{1}{\tau} \begin{cases} \sinh(t/\tau) e^{-\delta/\tau} & t \leq \delta \\ \sinh(\delta/\tau) e^{-t/\tau} & t > \delta \end{cases} \quad (4)$$

$\delta$  is the time delay between the two pulses, and  $\kappa_1$  and  $\kappa_2$  quantify the chance that the first and the second pulse lead to a photon detection event, respectively. Eqn (3) can be understood as the product of the probabilities (i) that the molecule is excited at time zero, (ii) that it emits a photon at time  $t_1$ , (iii) that the molecule is re-excited by a second pulse at time  $\delta$ , and (iv) that it emits a second photon at time  $t_1 + t$ . Generally, the values of  $\kappa_1$  and  $\kappa_2$  depend on the excitation pulse and detection polarization as well as the orientation of a molecule's excitation dipole. For a temporal distance between the two pulses that is much larger than the fluorescence decay time,  $\delta \gg \tau$ , and for lag time values much larger than the fluorescence decay time,  $t \gg \tau$ , this function approaches the simple form

$$F_1(t, \tau, \delta) \rightarrow \frac{1}{\tau} \exp\left(-\frac{|t-\delta|}{\tau}\right) \quad (5)$$

The chance to detect two photons with lag time  $t$  from *two different* molecules is similar to eqn (5), but with the distinction that the upper integration limit is now extended to infinity, leading to

$$\begin{aligned} & \int_{\min(\delta-t, 0)}^{\infty} dt_1 \frac{\kappa_1}{\tau} e^{-t_1/\tau} \frac{\kappa_2}{\tau} e^{-(t_1+t-\delta)/\tau} \\ &= \kappa_1 \kappa_2 \left[ F_1(t, \tau, \delta) + \frac{1}{2\tau} \exp\left(-\frac{t+\delta}{\tau}\right) \right] \\ &\equiv \kappa_1 \kappa_2 F_2(t, \tau, \delta) \end{aligned} \quad (6)$$

Eqn (6) is also the defining equation for  $F_2(t, \tau, \delta)$ .

The value of  $F_1(t, \tau, \delta)$ , in contrast to that of  $F_2(t, \tau, \delta)$ , tends to zero when the pulse delay  $\delta$  goes to zero, which is the essence of fluorescence antibunching, reflecting the fact that a single molecule cannot emit more than a single photon per excitation. However, the function  $F_1(t, \tau, \delta)$  does not take into account the rotational diffusion of the molecule (*i.e.* the rotation of its absorption/emission dipole). These contributions are contained in the pre-factors  $\kappa_1$  and  $\kappa_2$  in eqn (3) and will be considered in detail in the next sections.

### Rotational diffusion equation

The general theory of rotational diffusion of an anisotropic rotor can be found in several textbooks on quantum mechanics and was, in the context of correlation spectroscopy and light scattering, developed by Aragón and Pecora<sup>6</sup> (see also ref. 16). However, the mathematical approach presented there is highly involved. Thus, for the sake of completeness, we present here a brief review of the theory of rotational diffusion.

Let us start from the rotational diffusion equation

$$\frac{\partial P}{\partial t} = -(D_a \hat{J}_a^2 + D_b \hat{J}_b^2 + D_c \hat{J}_c^2) P \quad (7)$$

where  $a$ ,  $b$ , and  $c$  denote the principal axes of rotation of the molecule,  $P = P(\psi, \theta, \phi)$  is the probability of finding the molecule's principal axes rotated by Euler angles  $\psi$ ,  $\theta$  and  $\phi$  with respect to the lab frame,  $D_{a,b,c}$  are the generally different rotational diffusion coefficients around the molecule's principal axes, and  $\hat{J}_{a,b,c}$  are the three angular momentum operators around these axes. Eqn (7) is derived analogously to the more familiar translational diffusion equation. The difficulty with eqn (7) is that the angular momentum operators relate to the intrinsic frame of the molecule's principal axes which is rotating in time with respect to the fixed lab frame. To simplify matters, one can first rotate the molecule back to the lab's frame so that its axes align with the fixed Cartesian coordinate axes of the lab frame, then apply the operator, and finally rotate the molecule back, *i.e.*

$$\frac{\partial P}{\partial t} = -R(D_a \hat{J}_x^2 + D_b \hat{J}_y^2 + D_c \hat{J}_z^2) R^{-1} P \quad (8)$$

where  $R$  denotes the operation of rotating the molecule's frame from an orientation aligned with the lab's Cartesian  $x, y, z$ -coordinates to its actual orientation as specified by the Euler angles  $\phi$ ,  $\theta$  and  $\psi$ , see Fig. 1.

The rotation operator  $R$  can be decomposed into

$$R = R_z(\phi) R_y(\theta) R_x(\psi) \quad (9)$$

where  $R_{y,z}(\beta)$  denotes a rotation by angle  $\beta$  around axis  $y$  or  $z$ , respectively. The advantage of eqn (8) is that the angular momentum operators are now referring to the fixed lab frame.

To further analyze eqn (8), let us consider the special case that the function  $P$  is replaced by

$$P = R |l, m\rangle \quad (10)$$

where  $|l, m\rangle$  is an eigenfunction of the angular momentum operator obeying the two relations

$$\hat{J}^2 |l, m\rangle = (\hat{J}_x^2 + \hat{J}_y^2 + \hat{J}_z^2) |l, m\rangle = l(l+1) |l, m\rangle \quad (11)$$

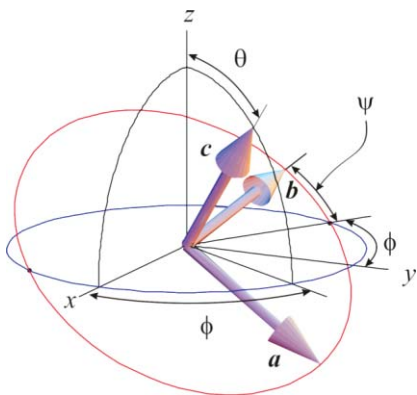


**Fig. 1** Geometric meaning of the three Euler angles  $\phi$ ,  $\theta$ , and  $\psi$ . Shown are the molecule's three principal (and orthogonal) axes of rotation  $a$ ,  $b$ , and  $c$ , and the three Cartesian axes  $x$ ,  $y$ , and  $z$  of the lab frame.

and

$$\hat{J}_z |l, m\rangle = m |l, m\rangle. \quad (12)$$

Inserting eqn (10) into eqn (8) yields

$$\frac{\partial(R|l, m\rangle)}{\partial t} = -R(D_a \hat{J}_x^2 + D_b \hat{J}_y^2 + D_c \hat{J}_z^2) |l, m\rangle. \quad (13)$$

Next, one has to clarify how the rotation operator  $R$  acts on  $|l, m\rangle$ . One of the most lucid derivations of this action is given by Feynman in ref. 17 using the possibility of representing any state  $|l, m\rangle$  through a combination of spin  $\frac{1}{2}$  states for which the transformation relations under action of  $R$  are well known, see *e.g.* chapter 3.3 in ref. 18. Here, we will give only the final result,

$$R(\phi, \theta, \psi) |l, m\rangle = e^{im\psi} \sum_{k=-l}^l e^{ik\phi} S_{mk}^l(\theta) |l, k\rangle. \quad (14)$$

The functions  $S_{mk}^l$  are Wigner's rotation matrices defined by

$$S_{mk}^l(\theta) = \langle l, k | R_y(\theta) | l, m \rangle = \left[ \frac{(j+k)!(j-k)!}{(j+m)!(j-m)!} \right]^{1/2} \times \sum_n \frac{(-1)^{j+k-n} (j+m)!(j-m)!}{k!(j+m-n)!(j+k-n)!(n-m-k)!} C^{2n-m-k} S^{2j+m+k-2n} \quad (15)$$

Here, we have introduced the abbreviations  $C = \cos(\theta/2)$  and  $S = \sin(\theta/2)$ .

For the sake of simplicity, we will further consider the special case of a symmetric top rotor where one has  $D_a = D_b = D_{\perp}$  and  $D_{\parallel} = D_c$ . The general case of the fully asymmetric rotor will be shortly discussed later. For the symmetric top rotor, one finds, by multiplying eqn (13) with  $\langle l, k |$ , that the functions

$$\exp\{-[D_{\perp}l(l+1) + (D_{\parallel} - D_{\perp})m^2]t\} C_{mk}^l(\phi, \theta, \psi) \quad (16)$$

with

$$C_{mk}^l(\phi, \theta, \psi) = c_{mk}^l \exp(ik\phi + im\psi) S_{mk}^l(\theta) \quad (17)$$

are *eigenfunctions* of the rotational diffusion equation. In eqn (17) we have introduced a normalizing factor  $c_{mk}^l$  so that  $C_{mk}^l(\phi, \theta, \psi)$  represents a complete orthonormal system of eigenfunctions obeying the relations

$$\int_0^{\pi} d\theta \sin\theta \int_0^{2\pi} d\phi \int_0^{2\pi} d\psi C_{mk}^l(\phi, \theta, \psi) C_{m'k'}^{l'*}(\phi, \theta, \psi) = \delta_{l,l'} \delta_{k,k'} \delta_{m,m'}. \quad (18)$$

$\delta_{l,l'}$  are Kronecker symbols taking the value one for  $l = l'$  and zero otherwise. The orthogonality of the functions  $C_{mk}^l(\phi, \theta, \psi)$  with respect to the variables  $\phi$  and  $\psi$  is obvious from their definition in eqn (17). The orthogonality with respect to  $\theta$  is less obvious, but is a consequence of the fundamental orthogonality theorem of group theory (see *e.g.* ref. 19) which is applied here to the functional representation of the three-dimensional rotation group as given by the functions  $C_{mk}^l(\phi, \theta, \psi)$ . With this complete orthonormal system of eigenfunctions, the probability that a molecule has rotated, within time  $t$ , from an initial orientation  $\Omega'$  described by the Euler angles  $\phi'$ ,  $\theta'$  and  $\psi'$  into a final orientation  $\Omega$  described by Euler angles  $\phi$ ,  $\theta$  and  $\psi$  is given by Green's function in the standard way<sup>20</sup> as

$$G(\Omega, \Omega', t) = \sum_{l=0}^{\infty} \sum_{m,k=-l}^l \exp\{-[D_{\perp}l(l+1) + (D_{\parallel} - D_{\perp})m^2]t\} \times C_{mk}^l(\phi, \theta, \psi) C_{m'k'}^{l'*}(\phi', \theta', \psi'), \quad (19)$$

where a star superscript denotes complex conjugation.

For the sake of completeness, we will briefly discuss the most general case of a completely asymmetric rotor. Now, it is not possible to obtain simple eigenfunctions of the form of eqn (7). However, it is helpful to introduce the operators

$$\hat{J}_{\pm} = \hat{J}_x \pm i\hat{J}_y \quad (20)$$

so that the  $\hat{J}_x$  and  $\hat{J}_y$  operators on the right hand side of eqn (8) can be written as

$$\hat{J}_x^2 = \frac{1}{4}(\hat{J}_+^2 + \hat{J}_-^2 + \hat{\mathbf{J}}^2 - \hat{J}_z^2 + \hat{J}_z) \quad (21)$$

and

$$\hat{J}_y^2 = \frac{1}{4}(-\hat{J}_+^2 - \hat{J}_-^2 + \hat{\mathbf{J}}^2 - \hat{J}_z^2 + \hat{J}_z) \quad (22)$$

where the commutation property of the angular momentum operators

$$[\hat{J}_x, \hat{J}_y] \equiv \hat{J}_x \hat{J}_y - \hat{J}_y \hat{J}_x = i\hat{J}_z \quad (23)$$

has been used. When taking into account how the operators  $\hat{J}_{\pm}$  act on the eigenstates  $|l, m\rangle$  (see, for example, chapter 3.4 in ref. 18):

$$\hat{J}_{\pm} |l, m\rangle = \sqrt{l(l+1) - m(m\pm 1)} |l, m\pm 1\rangle \quad (24)$$

it is straightforward to see that eqn (8) separates, for each value of  $l$ , into a set of  $2l + 1$  coupled ordinary and linear differential equations on the basis of the  $2l + 1$  state vectors  $|l, m\rangle$  (more correctly, into two sets of equations with  $l + 1$  equations coupling the values of  $m$  with  $m \in [-l, -l + 2, \dots, l]$  and  $l$  equations coupling the values of  $m$  with  $m \in [-l + 1, -l + 3, \dots, l - 1]$ , which can be solved in a standard way.<sup>21</sup> This yields  $2l + 1$  orthonormal eigenfunctions as superpositions of the states  $|l, m\rangle$  with corresponding eigenvalues as characteristic temporal exponents, from which Green's function can be constructed as before. Because the case of a fully asymmetric rotor is of rather little interest for almost all fluorescence-based measurements of molecular rotation, we will not pursue this topic further.

## Excitation and detection

After having found Green's function for the rotation diffusion equation, we have to specify the fluorescence excitation and detection conditions of the measurement, in particular its polarization properties. Let us assume that the fluorescence lifetime is considerably shorter than the rotational diffusion time, which is mostly the case when studying rotational diffusion of large proteins by using short-lifetime dyes. Then, we need only to consider the so-called molecule detection function (MDF) describing the chance to excite and detect a photon for a dye molecule with a given orientation and position in sample space. The calculation of this function can be done using a wave-optics approach as described in ref. 22. For our further considerations it is important that the MDF can be expanded into a series of spherical harmonics in the angles  $\alpha$  and  $\beta$  which describe the angular orientation  $\omega$  of the excitation/emission dipole (which are assumed to be collinear) as depicted in Fig. 2. The coefficients of this series expansion are functions of the molecule's position  $\mathbf{r}$ , and the MDF, which will be denoted by  $U(\alpha, \beta, \mathbf{r})$ , is thus represented through

$$U(\omega, \mathbf{r}) \equiv U(\alpha, \beta, \mathbf{r}) = \sum_{l=0}^{\infty} \sum_{m=-l}^l u_{lm}(\mathbf{r}) Y_{lm}(\beta, \alpha) \quad (25)$$

where the spherical harmonics  $Y_{lm}(\beta, \alpha)$  are defined by

$$Y_{lm}(\beta, \alpha) = P_l^m(\cos \beta) \exp(im\alpha). \quad (26)$$

Here, the functions  $P_l^m(\cos \beta)$  are associated Legendre polynomials.<sup>23</sup> Using the orthogonality of spherical harmonics, the coefficients  $u_{lm}(\mathbf{r})$  can be found from the full MDF *via* the backward transformation

$$u_{lm}(\mathbf{r}) = \int_0^{\pi} d\beta \sin \beta \int_0^{2\pi} d\alpha U(\beta, \alpha, \mathbf{r}) Y_{lm}^*(\beta, \alpha) \quad (27)$$

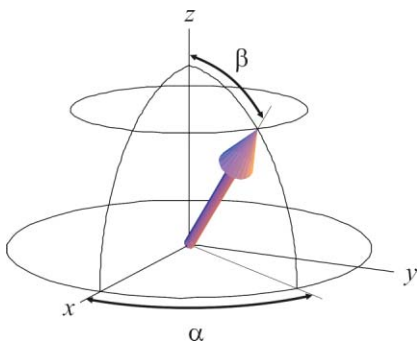


**Fig. 2** Geometric meaning of the orientation angles  $\beta$  and  $\alpha$  with respect to the lab frame.

The importance of representation (25) lies in the fact that the spherical harmonics themselves are representations of the three-dimensional rotation group and transform under rotation according to eqn (14). The MDF depends, of course, on the peculiarities of the excitation, and can be different for different excitation pulses (for example, when exciting the sample with a pulse train of pulses with alternating polarization). A first laser pulse with corresponding MDF  $U_1(\omega, \mathbf{r})$  thus 'prepares' the sample in such a way that  $U_1(\omega, \mathbf{r})$  describes the chance to detect a photon from an excitation/emission dipole at position  $\mathbf{r}$  having

orientation  $\omega$ . A next important thought is that we are interested in measurements where the protein is tagged with a dye molecule in such a way that the relative orientation of the dye with respect to the protein's principal axes is *random* but fixed (co-rotation of dye with protein). Thus, rotating the distribution  $U_1(\omega, \mathbf{r})$  back into the protein's frame of principal axes which has orientation  $\Omega'$  with respect to the lab frame gives the average chance to excite and detect a photon from the protein-dye complex. Next, Green's function  $G(\Omega, \Omega', t)$ , eqn (19), gives the chance that the protein-dye complex rotates from orientation  $\Omega'$  into orientation  $\Omega$  within time  $t$ , and, by a similar argument as before, the chance to excite and detect a photon by a second laser pulse with MDF  $U_2(\omega, \mathbf{r})$  is given by a back-rotation  $\Omega$  of  $U_2(\omega, \mathbf{r})$  into the protein's frame. Finally, by integrating over all possible positions and orientations, one obtains the average of the product  $\kappa_1 \kappa_2$  (averaged over many repeats of the double-pulse excitation and many different relative protein-dye orientations) that we need for proceeding with eqn (5) and (6):

$$\langle \kappa_1 \kappa_2 \rangle_t = \int d\mathbf{r} \int d\omega \int d\Omega \int d\Omega' [R^{-1}(\Omega) U_2(\omega, \mathbf{r})] \times G(\Omega, \Omega', t) [R^{-1}(\Omega') U_1(\omega, \mathbf{r})] \quad (28)$$

where  $R^{-1}$  is the back-rotation operator. The integrations run over all possible initial and final orientations  $\Omega'$  and  $\Omega$  of the protein, all possible dye-label orientations  $\omega$ , and all possible positions  $\mathbf{r}$ . It should be emphasized that the above expression is quite general, allowing for different excitation and detection geometries/polarizations for the first and second laser pulse. Now, using the transformation relation (14), and the orthonormality of the eigenfunctions  $C_{mk}^l(\phi, \theta, \psi)$  and of spherical harmonics  $Y_{lm}$ , the integrations over  $\Omega$ ,  $\Omega'$  and  $\omega$  can be performed analytically, resulting in

$$\langle \kappa_1 \kappa_2 \rangle_2 = \sum_{l=0}^{\infty} \sum_{m=-l}^l \left[ \int d\mathbf{r} u_{2,lm}^*(\mathbf{r}) u_{1,lm}(\mathbf{r}) \right] \times \exp[-l(l+1)D_{\perp}t - (D_{\parallel} - D_{\perp})m^2] \quad (29)$$

For a spherically symmetric molecule with  $D_{\perp} = D_{\parallel} \equiv D$  this expression simplifies to

$$\langle \kappa_1 \kappa_2 \rangle_t = \sum_{l=0}^{\infty} \left[ \sum_{m=-l}^l \int d\mathbf{r} u_{2,lm}^*(\mathbf{r}) u_{1,lm}(\mathbf{r}) \right] \exp[-l(l+1)Dt] \quad (30)$$

The explicit calculation of the coefficients  $u_{\alpha,lm}(\mathbf{r})$  is a formidable task, and for the details the reader is referred to ref. 22 and citations therein. Remarkably, when neglecting optical saturation (*i.e.* excitation rate is directly proportional to the absolute square of the scalar product of the excitation light electric field amplitude times the molecule's absorption dipole vector), only coefficients with  $l = (0, 2, 4)$  will differ from zero. Even taking into account depolarization in excitation and detection caused by objectives with high numerical aperture<sup>24,25</sup> does not change the computation noticeably. As an example, Fig. 3 shows the result of a numerical calculation for a 1.2 N.A. water immersion objective as a function of the laser beam diameter coupled into the objective's back focal plane. In these calculations, it was assumed that detection is done by *two detectors looking at orthogonal emission polarizations*. Without loss of generality, we will denote the detection polarization for the first photon by the symbol  $\parallel$ , and that for the second photon

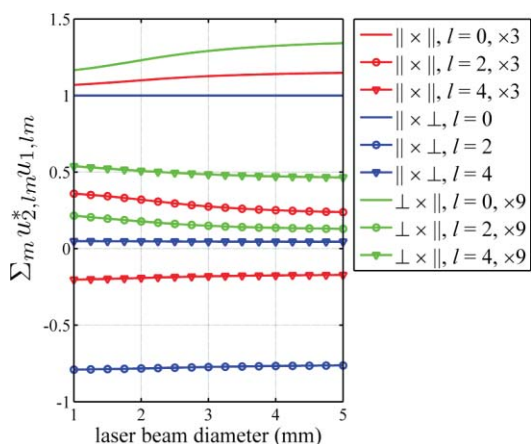


**Fig. 3** Dependence of the (normalized) coefficients  $[\sum_m \int dr u_{2,lm}^* u_{1,lm}]$  in eqn (30) for  $l = 0$  (solid lines),  $l = 2$  (solid lines with circles),  $l = 4$  (solid lines with triangles) and for different excitation/detection polarizations as a function of laser beam diameter (measured at the objective's back focal plane). It is assumed that detection is done through two polarizers with orthogonally aligned polarization axes for the first and the second photon. The red curves show the case when the first and second laser pulse are both polarized along the same direction as the first or the second detector polarizer; the blue curves show the case when both laser pulses have the same polarization as the corresponding detector polarizers; and the green curves show the case when both laser pulses are polarized perpendicular to the corresponding detector polarizers. The calculations were done for a perfectly aplanatic 1.2 N.A. water immersion objective.

by  $\perp$  ( $\parallel \times \perp$  detection polarization mode). Then, there are three principally different excitation modes: (i) polarization of excitation for the first and second photon is both parallel to the respective detection polarization ( $\parallel \times \perp$  excitation polarization mode), (ii) polarization of excitation for the first and second photon is both orthogonal to the respective detection polarization ( $\perp \times \parallel$  excitation polarization mode), and (iii) excitation polarization for both photons is the same ( $\parallel \times \parallel$  or  $\perp \times \perp$  excitation polarization mode), so that the first (second) photon is excited with an excitation polarization parallel to its detection polarization, and the second (first) orthogonally to its detection polarization.

Fig. 3 shows several remarkable features: Firstly, the amplitude ratios in the  $\parallel \times \perp$ , the  $\perp \times \parallel$  and the  $\parallel \times \parallel$  excitation mode are close to 9 : 1 : 3 for  $l = 0$ , (-18) : 1 : 3 for  $l = 2$ , and (-6) : 8 : 9 for  $l = 4$ , which are the values in the limit of zero numerical aperture, the situation considered by Aragón and Pecora.<sup>6</sup> Secondly, one has always non-zero contributions with  $l = 4$ . However, the relative weight of these contributions when compared to the  $l = 2$  term is smallest for the  $\parallel \times \perp$  excitation mode, where it is *ca.* 1/15th of the amplitude for  $l = 2$ . Thirdly, when getting closer to diffraction-limited focusing (values at the right end of Fig. 3), depolarization effects have a non-negligible impact on the different pre-exponential amplitudes in eqn (29). The lowest impact is observed for the  $\parallel \times \perp$  excitation mode, which makes this mode of excitation/detection the most favorable one for measuring rotational diffusion *via* fluorescence correlation spectroscopy in a confocal microscope with high N.A. It yields maximum amplitude of the lag-time dependent part of the correlation function with smallest contribution from the  $l = 4$  mode and smallest impact from depolarization effects. As an example, the modeled correlation functions for a globular protein

(isotropic rotor) with 20 ns rotational diffusion time  $\tau_{\text{rot}} = 1/6D_{\text{rot}}$  are shown in Fig. 4.

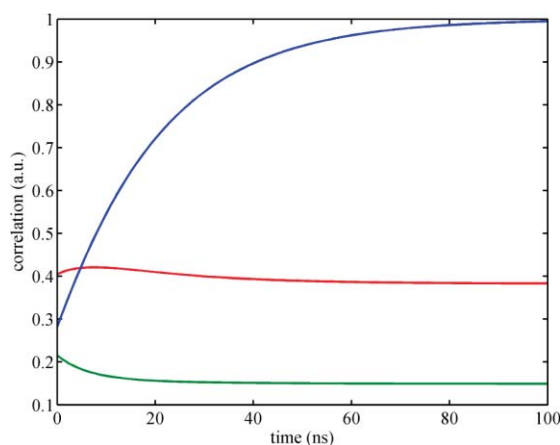


**Fig. 4** Correlation functions for  $\parallel \times \perp$  (blue),  $\perp \times \parallel$  (green) and  $\parallel \times \parallel$  (red) excitation mode for a spherical globular protein with 20 ns rotational diffusion time.

Often, fluorescent molecules exhibit a non-negligible angle between absorption and emission dipole. This will change the amplitudes of the different exponential terms in the autocorrelation function, but not the exponents themselves. Because our data analysis of autocorrelation curves for obtaining rotational diffusion values will solely rely on these exponents, we will not consider here how a finite angle between absorption and emission dipole will modify the pre-exponential amplitudes.

### Molecular shape and rotational diffusion

In this section we will briefly consider when it is necessary to take into account the non-spherical shape of a molecule, and when the assumption of a rotationally symmetric shape is still sufficient. As already noted, any molecule can be modeled by an object with three orthogonal axes of rotation (principal axes) with, in the most general case, three different rotational diffusion constants around each of these axes. In almost all cases of practical interest, it is sufficient to approximate a molecule by a symmetric top, *i.e.* an object that has two identical rotational diffusion constants around two of its principal axes and one different around the third. This corresponds to approximating the shape of a molecule by a prolate or oblate ellipsoid of rotation. The question is how large the axis ratio between the axes of the ellipsoid has to be so that it is clearly discernible in a rotational diffusion measurement. Following Perrin<sup>26,27</sup> and Koenig,<sup>28</sup> the rotational diffusion coefficients for an oblate ellipsoid of rotation with aspect ratio  $\varepsilon = R_{\perp}/R_{\parallel} < 1$  are given by

$$\frac{D_{\parallel}}{D_0} = \frac{3\varepsilon^2}{2(1-\varepsilon^4)} \left\{ \frac{2-\varepsilon^2}{\sqrt{1-\varepsilon^2}} \ln \left[ \frac{1+\sqrt{1-\varepsilon^2}}{\varepsilon} \right] - 1 \right\} \quad (31)$$

and

$$\frac{D_{\perp}}{D_0} = \frac{3}{2(1-\varepsilon^2)} \left\{ 1 - \frac{\varepsilon^2}{\sqrt{1-\varepsilon^2}} \ln \left[ \frac{1+\sqrt{1-\varepsilon^2}}{\varepsilon} \right] \right\} \quad (32)$$

whereas for a prolate ellipsoid of rotation ( $\varepsilon > 1$ ) they read

$$\frac{D_{\parallel}}{D_0} = \frac{3\varepsilon^2}{2(\varepsilon^4 - 1)} \left\{ \frac{\varepsilon^2 - 2}{\sqrt{\varepsilon^2 - 1}} \arctan(\sqrt{\varepsilon^2 - 1}) + 1 \right\} \quad (33)$$

and

$$\frac{D_{\perp}}{D_0} = \frac{3}{2(\varepsilon^4 - 1)} \left\{ \frac{\varepsilon^2}{\sqrt{\varepsilon^2 - 1}} \arctan(\sqrt{\varepsilon^2 - 1}) - 1 \right\} \quad (34)$$

Here,  $D_0$  is the diffusion coefficient of a sphere of radius  $R_0$  with the same volume as the ellipsoid, *i.e.*

$$R_0^3 = R_{\parallel} R_{\perp}^2, \quad (35)$$

and the value of  $D_0$  is given by eqn (2). In all the above expressions, the subscript  $\parallel$  refers to the symmetry axis, and the subscript  $\perp$  to the two transversal axes of the ellipsoid. Fig. 5 shows the dependence of the two rotational diffusion coefficients on the eccentricity  $\varepsilon$  of the ellipsoid. As can be seen, the values of rotational diffusion coefficients change quite quickly with changing eccentricity. Theoretically, it should be possible to observe the difference in the rotational diffusion coefficients around the symmetry and the transverse axes by the emergence of a more complex multi-exponential behavior of the correlation function compared to the correlation function produced by an ideal spherical rotor.

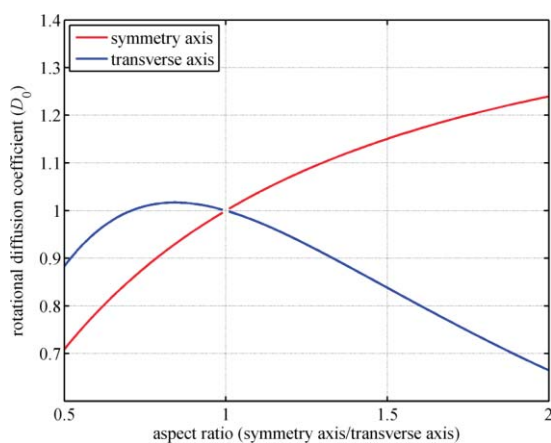


**Fig. 5** Dependence of the rotational diffusion coefficients on ellipsoid eccentricity.

However, in practice the measured correlation curves are usually too noisy to extract that information if the axis ratio becomes not exceedingly large. Usually one fits the correlation function assuming a spherically-shaped molecule and obtains a *mean* rotational diffusion coefficient and a *mean* hydrodynamic radius. This corresponds to taking the mean of the diffusion coefficients,  $\langle D \rangle = (2D_{\perp} + D_{\parallel})/3$ , and to use eqn (2) for obtaining the hydrodynamic radius. Due to the cubic relationship between radius and diffusion coefficient, the dependence of the thus-defined mean value of hydrodynamic radius changes much less with eccentricity than the individual rotational diffusion coefficients. This is shown in Fig. 6, where one can see that the mean value of the hydrodynamic radius changes only slightly in the range of  $0.75 < \varepsilon < 1.5$  at maximum by only 2%. Thus, assuming a spherical shape is a quite reasonable approach for moderate values of eccentricity. We will use this assumption when measuring the rotational diffusion of globular proteins.

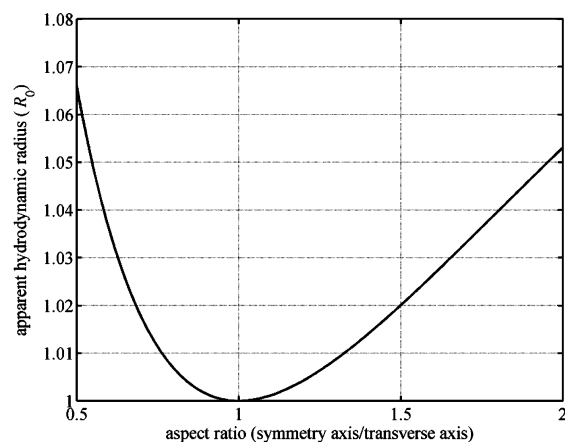


**Fig. 6** Dependence of the mean hydrodynamic radius on ellipsoid eccentricity.

## Materials and methods

### Fluorescent labeling

BSA and HSA (Sigma-Aldrich) were nonspecifically labeled with Alexa Fluor® 647 succinimidyl ester (Invitrogen GmbH, Karlsruhe, Germany). This dye was chosen for two reasons. Firstly, it has a rather short fluorescence lifetime of *ca.* 1.2 ns, assuring that the fluorescence excited by one laser pulse decays completely before the next excitation pulse (for the inter-pulse time distances as used in the present study, see below). Secondly, the dye is rather hydrophobic which leads to its co-rotation with BSA and HSA (as was checked by static anisotropy measurement). However, for the two other proteins used in this study, aldolase and ovalbumin (gel filtration calibration kit HMW, GE Healthcare), the hydrophobic properties of Alexa647 were not enough to assure its co-rotation with the protein. Therefore, these proteins were labeled with Cy5 bis-succinimidyl ester (GE Healthcare Europe GmbH, Freiburg, Germany). The two succinimidyl ester groups can non-specifically react with *two* solvent-exposed lysins on a protein's surface, assuring a fixed orientation of the dye with respect to the labeled protein. Furthermore, Cy5 also has a short fluorescence lifetime of 1 ns, assuring complete decay of fluorescence between laser pulses.

Labeled proteins were purified using an HPLC system (Jasco Labor und Datentechnik GmbH, Groß-Umstadt, Germany), then kept in phosphate buffered saline (PBS) at pH 7.4, and were used for the measurements directly after preparation.

### Measurement set-up

All measurements were done with a commercial confocal microscopy system (MicroTime 200 with dual-focus option, Pico-Quant GmbH, Berlin, Germany) which is similar to the set-up described in detail in ref. 2. In summary, the light of two identical, linearly polarized pulsed diode lasers (wavelength 640 nm, pulse duration 50 ps fwhm) is combined by a polarizing beam splitter. Both lasers are pulsed synchronously with a repetition rate of 80 MHz. Inserting a time delay of  $\sim 6$  ns (Ortec Delay 425, AME-TEK GmbH, Meerbusch, Germany) between the pulse trains of the first and second laser creates a pulsed interleaved excitation (or PIE<sup>29</sup>) with about 6 ns spaced pulses of alternating polarization. Both beams are coupled into a polarization-maintaining single

mode fiber. At the fiber output, the light is collimated and reflected by a dichroic mirror towards the microscope's objective (UPLSAPO 60× W, 1.2 N.A., Olympus Deutschland GmbH, Hamburg, Germany).

Fluorescence is collected by the same objective (epi-fluorescence setup), passed through the dichroic mirror, and focused onto a single circular aperture (diameter 150 μm). After the pinhole, the light is collimated, split by a polarizing beam splitter cube and focused onto two single-photon avalanche diodes (SPCM-AQR-13, PerkinElmer Optoelectronics, Wiesbaden, Germany). Single-photon counting electronics (HydraHarp 400, PicoQuant GmbH, Berlin, Germany) independently records the detected photons of both detectors with an absolute temporal resolution of two picoseconds on a common time frame.

All measurements were done in Lab-Tek II chambered cover-glass systems (Nunc Thermo Electron LED GmbH, Langensfeld, Germany) coated with BSA to prevent unspecific adsorption of the labeled proteins. Sample temperature was controlled with a HH500 digital thermometer (Omega Newport Electronics GmbH, Deckenpfronn, Germany). The values of the rotational diffusion coefficient and resulting hydrodynamic radius were subsequently recalculated for a temperature of 20 °C employing eqn (2), and using the known dependency of water's dynamic viscosity on temperature.

### Calculation of the ACF

As described in the theory section, the most advantageous mode of measuring an ACF for determining rotational diffusion is to calculate it from photon pairs excited with laser pulses of crossed polarization and detected with two detectors having detection polarization collinear to the corresponding excitation pulses. This is relatively easy to achieve with the experimental set-up and the described measurement mode. To better understand that, consider the TCSPC histograms as recorded by both detectors in our set-up, which are shown in Fig. 7. As can be seen, each detector observes two consecutive fluorescence decays within a complete excitation cycle: one with a large and one with a small amplitude. The large amplitude decay corresponds to a laser pulse polarization collinear with the detection polarization, whereas the small amplitude decay corresponds to a laser pulse polarization orthogonal to the detection polarization. Thus, by inspecting the TCSPC histograms, one can precisely determine the relative polarizations of the exciting laser pulse with respect to the detection polarization.

Using fluorescence dyes showing fluorescence decay times sufficiently short so that their fluorescence has nearly completely decayed until the next laser pulse occurs, and exploiting the TCSPC information of each photon, one can unequivocally associate each detected photon to the laser pulse which had excited it, similarly to what is done in pulsed interleaved excitation<sup>29</sup> or dual-focus FCS.<sup>2</sup>

Now, having the ability to determine, for each detected photon, the polarization of its exciting laser pulse, and the polarization of its detector, it is straightforward to calculate the desired  $\parallel \times \perp$  polarization ACF by correlating all photon pairs where the first photon is excited by a  $\parallel$  polarized laser and detected by the detector with  $\parallel$  detection polarization, and the second photon is excited by a laser pulse with  $\perp$  polarization and detected by the detector with

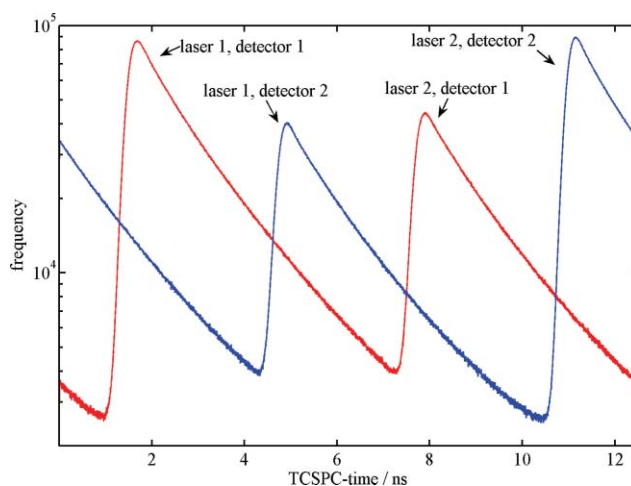


**Fig. 7** Red curve shows TCSPC-histogram of photons detected by detector #1, in blue is the corresponding curve for detector #2. The maxima at  $\sim 1.75$  ns (detector #1) and  $\sim 11.5$  ns (detector #2) correspond to laser pulses with their polarization collinear with the detection polarization. The local maxima at 8.0 ns (detector #1) and 5.25 ns (detector #2) correspond to laser pulses with their polarization orthogonal to the detection polarization.

$\perp$  detection polarization. This computation is done using a general algorithm of calculating an ACF on the basis of asynchronous photon counting data as described in ref. 30.

At this point it is useful to realize that for extracting the rotational diffusion information from the ACF it is not necessary to compute the ACF with a temporal resolution better than that which is given by the laser pulse distances. Therefore, we associate each detected photon with a 'virtual' detection time equal to the time of its exciting laser pulse. By doing that, the resulting correlation function loses all information connected with the fluorescence decay, but maintains the rotational diffusion information. A resulting ACF is shown in Fig. 8, where the bar plot shows values only at the discrete lag times corresponding to all possible time intervals between orthogonal and horizontal laser pulses. Here, ACF values for  $t > t_0$  correspond to photon pairs where the first photon is detected by the detector #1 and the second by detector #2, and ACF values for  $t < t_0$  to the

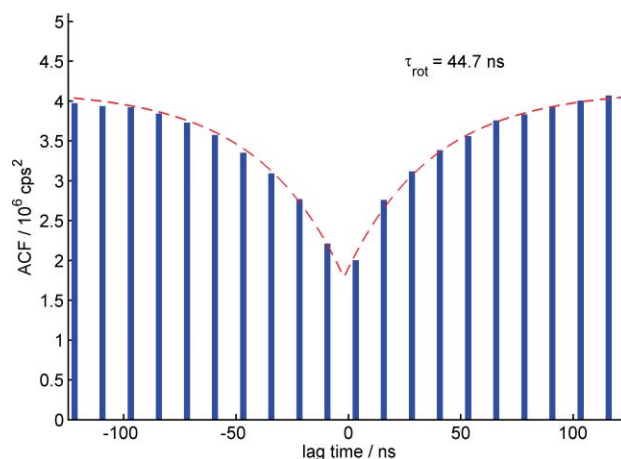


**Fig. 8** Measured  $\parallel \times \perp$  correlation function (blue bars) and fitted mono-exponential lag-time dependence (dashed red line) for HSA.

reverse order of detection, where  $t_0$  is some absolute time offset determined by the relative temporal position of the laser pulse trains with respect to the internal clock of the photon counting electronics. Of course, for both  $t > t_0$  and  $t < t_0$ , only photon pairs are correlated where the pulse polarization is collinear with detection polarization. The representation of the ACF as shown in Fig. 8 considerably simplifies its evaluation, because the visible temporal dynamics is only due to rotational diffusion but not to fluorescence decay.

Fitting is done with a mono-exponential function of the form

$$A + B \exp[-6D|t - t_0|] \quad (36)$$

where  $A$  and  $B$  are some amplitude factors, and  $D$  is the rotational diffusion coefficient. By adopting this fit function we assume that the studied molecules are close to spherically symmetric, and that all terms with  $l > 2$  in eqn (30) are negligible compared with the  $l = 2$  term.

## Results and discussion

First, we measured the rotational diffusion of HSA non-specifically labeled with Alexa Fluor® 647. Fig. 8 shows the ACF for the  $\parallel \times \perp$  excitation mode, calculated as described in the previous section. The data are fitted with the mono-exponential model curve of eqn (36), the exponent of which yields the inverse rotational diffusion time,  $\tau_{\text{rot}} = 1/6D_{\text{rot}}$ . As can be seen, the fit quality is remarkably good, although we assumed spherical symmetry of the protein and neglected any terms with  $l = 4$ . This exemplifies once more that the  $l = 4$  contribution to the correlation function in  $\parallel \times \perp$  excitation mode is indeed negligibly small.

To check the dependence of the obtained rotational diffusion time  $\tau_{\text{rot}}$  on total measurement time, we partitioned the measured photon stream into subsets of different measurement times, calculated for each subset the correlation function, fitted the rotational diffusion time, and averaged these values over subsets of equal duration. The resulting values of  $\tau_{\text{rot}}$  and their standard deviation (if the total amount of data could be divided into more than two subsets for the given duration) are shown in Fig. 9. As can be seen, the obtained value of rotational diffusion quickly approaches a fixed value if the measurement time becomes larger than  $\sim 2000$  s. Because the average photon count rate of our measurement was  $\sim 43$  kcps (both detectors), this corresponds to a value  $\sim 10^8$  measured photons.

Using the Stokes–Einstein–Debye equation, eqn (2), and the known values of temperature and viscosity, our determined rotational diffusion value corresponds to a value of the hydrodynamic radius  $R_{\text{rot}}$  of  $(3.4 \pm 0.2)$  nm.

Next, we measured the rotational diffusion of the protein bovine serum albumin (BSA), again non-specifically labeled with Alexa Fluor® 647. The resulting ACF is shown in Fig. 10, together with a mono-exponential fit.

The dependence of the obtained value on measurement time was similar to that for BSA, and the finally obtained hydrodynamic radius is  $(3.5 \pm 0.2)$  nm, which is in good agreement with literature values for BSA ( $R_{\text{rot}} = 3.4$  nm in ref. <sup>31</sup>, and  $R_{\text{rot}} = 3.5$  nm according to ref. <sup>32</sup>), where it was measured *via* fluorescence anisotropy. In an extended study,<sup>33</sup> Ferrer *et al.* recently combined both fluorescence anisotropy measurements with theoretical modeling to elucidate the anisotropic shape of BSA in solution. They found an average

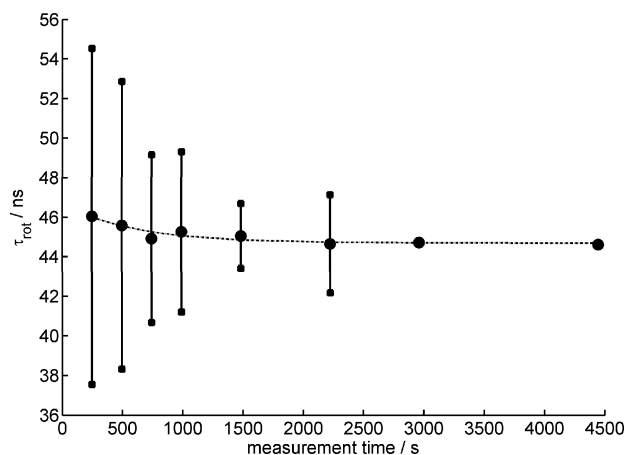


**Fig. 9** Dependence of the determined values of rotational diffusion on measurement time. The dotted line shows an exponentially decaying asymptotic fit to the determined values.

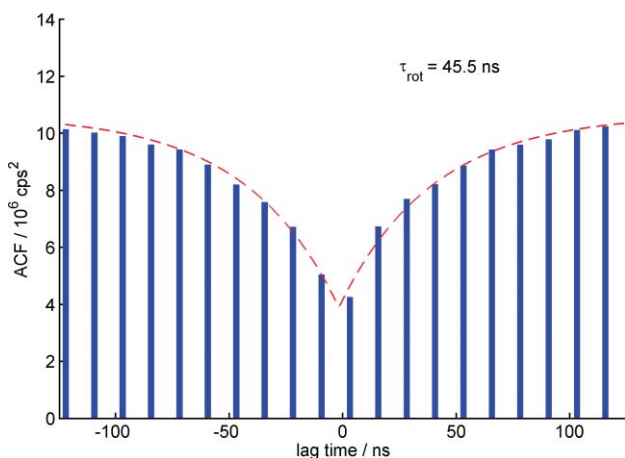


**Fig. 10** Measured  $\parallel \times \perp$  correlation function (blue bars) and fitted mono-exponential lag-time dependence (dashed red line) for BSA.

radius value of  $\sim 3.75$  nm, which is still in reasonable agreement with our value here.

Finally, we tried to measure the rotational diffusion of the non-specifically labeled proteins aldolase and ovalbumin. Here, the label Alexa Fluor® 647 is not “sticky” enough to co-rotate with the proteins. It is assumed that the hydrophobicity of BSA accidentally assured such a co-rotation, but that it is not granted when labeling arbitrary proteins. Thus, we chose the bifunctional fluorescence label Cy5 bis-succinimidyl ester for non-specifically labeling aldolase and ovalbumin. By fluorescence anisotropy measurements we checked that this label indeed co-rotates with the proteins. The measured ACFs are presented in Fig. 11 and 12. For these two proteins, fit quality was also excellent, and the extracted hydrodynamic radius values are  $(4.1 \pm 0.1)$  nm for aldolase and  $(2.8 \pm 0.1)$  nm for ovalbumin. For both proteins, we observed a similar dependence of fitted values on measurement time as those observed for BSA.

Table 1 summarizes all our results on the hydrodynamic radii of the studied proteins, and compares it with literature values (as far as they were available) as well as with theoretical predictions by HydroPro 7c.<sup>35</sup> There is no theoretical value for BSA, because no crystal structure is known for that protein.

**Table 1** Comparison of our measured values of hydrodynamic radius with published literature values and theoretical values calculated using the structural information from protein database (entry indicated in brackets) and the program HydroPro 7c;<sup>35</sup> the last column gives the molecular weight of the protein

Protein	$R_{\text{rot}}/\text{nm}$		HydroPro 7c	MW/kDa
	FCS	Literature		
HSA	$3.4 \pm 0.2$		3.6 (1bm0)	69.4
BSA	$3.5 \pm 0.2$	3.4 <sup>31</sup> 3.5 <sup>32</sup> 3.7 <sup>33</sup>	Not available	Not available
Ovalbumin	$2.8 \pm 0.1$	3.2 <sup>34</sup>	3.1 (1vac)	44.2
Aldolase	$4.1 \pm 0.1$		4.9 (1zah)	156.8

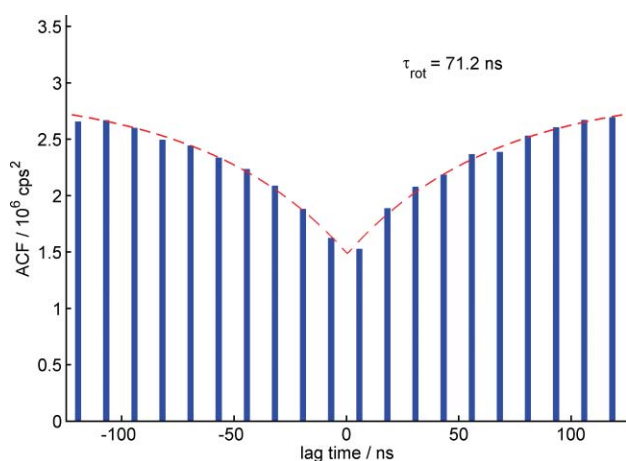


**Fig. 11** Measured  $\parallel \times \perp$  correlation function (blue bars) and fitted mono-exponential lag-time dependence (dashed red line) for aldolase.

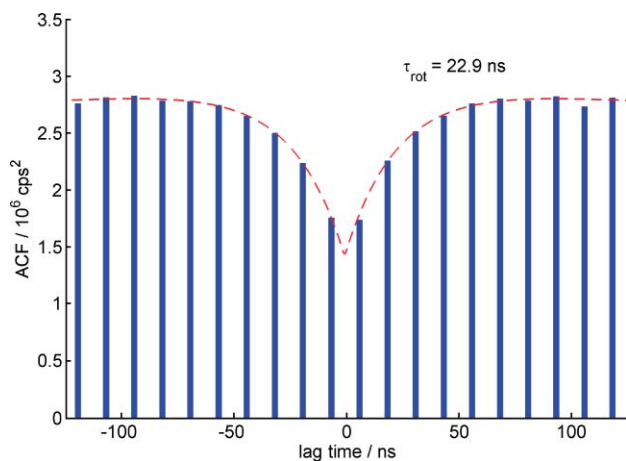


**Fig. 12** Measured  $\parallel \times \perp$  correlation function (blue bars) and fitted mono-exponential lag-time dependence (dashed red line) for ovalbumin. Due to a slight shift of the relative temporal position of the  $\parallel$  laser pulse train to the  $\perp$  laser pulse train (as compared with the other measurements in Fig. 8, 10, and 11), no antibunching is visible here.

## Conclusions

We presented a new variant of fluorescence correlation spectroscopy to measure rotational diffusion of macromolecules. Our approach ensures (i) a maximum amplitude of the rotational-diffusion related contribution in the correlation function, (ii) a

minimum impact of higher order ( $l = 4$ ) contributions, allowing for a mono-exponential fitting of the rotational diffusion time, and (iii) it works best for rotational diffusion times that are large compared to the fluorescence decay time, exactly the situation when fluorescence anisotropy will no longer be useful. Thus, we hope that fluorescence correlation spectroscopy on the nanosecond timescale will become an efficient and reliable method for measuring rotational diffusion of large macromolecules.

## Acknowledgements

We are grateful to the Deutsche Volkswagenstiftung and the Deutsche Forschungsgemeinschaft for their financial support.

## Notes and references

- 1 A. Einstein, *Investigations on the Theory of the Brownian Movement*, Dover, New York, 1985.
- 2 T. Dertinger, V. Pacheco, I. von der Hocht, R. Hartmann, I. Gregor and J. Enderlein, Two-Focus Fluorescence Correlation Spectroscopy: A New Tool for Accurate and Absolute Diffusion Measurements, *ChemPhysChem*, 2007, **8**, 433–443.
- 3 P. Debye, *Polar Molecules*, The Chemical Catalogue Company, New York, 1929, pp. 77–108.
- 4 J. R. Lakowicz, *Principles of Fluorescence Spectroscopy*, Kluwer Academic/Plenum Publishers, New York, 1999, pp. 291–320.
- 5 M. Ehrenberg and R. Rigler, Rotational brownian motion and fluorescence intensity fluctuations, *Chem. Phys.*, 1974, **4**, 390–401.
- 6 S. R. Aragón and R. Pecora, Fluorescence correlation spectroscopy and Brownian rotational diffusion, *Biopolymers*, 1975, **14**, 119–138.
- 7 P. Kask, P. Piksarv, Ü. Mets, M. Pooga and E. Lippmaa, Fluorescence correlation spectroscopy in the nanosecond time range: rotational diffusion of bovine carbonic anhydrase B, *Eur. Biophys. J.*, 1987, **14**, 257–261.
- 8 J. M. Tsay, S. Dose and S. Weiss, Rotational and Translational Diffusion of Peptide-Coated CdSe/CdS/ZnS Nanorods Studied by Fluorescence Correlation Spectroscopy, *J. Am. Chem. Soc.*, 2006, **128**, 1639–1647.
- 9 S. Felekyan, R. Kühnemuth, V. Kudryavtsev, C. Sandhagen, W. Becker and C. A. M. Seidel, Full correlation from picoseconds to seconds by time-resolved and time-correlated single photon detection, *Rev. Sci. Instrum.*, 2005, **76**, 083104.
- 10 M. Tabak, D. de Sousa Neto and C. E. G. Salmon, On the Interaction of Bovine Serum Albumin (BSA) with Cetyltrimethyl Ammonium Chloride Surfactant: Electron Paramagnetic Resonance (EPR) Study, *Braz. J. Phys.*, 2006, **36**, 83–89.
- 11 P. Kask, P. Piksarv and Ü. Mets, Fluorescence correlation spectroscopy in the nanosecond time range: Photon antibunching in dye fluorescence, *Eur. Biophys. J.*, 1985, **12**, 163–166.
- 12 W. P. Ambrose, P. M. Goodwin, J. Enderlein, D. J. Semin, J. C. Martin and R. A. Keller, Fluorescence photon antibunching from single molecules on a surface, *Chem. Phys. Lett.*, 1997, **269**, 365–370.
- 13 P. Tinnefeld, K. D. Weston, T. Vosch, M. Cotlet, T. Weil, J. Hofkens, K. Müllen, F. C. de Schryver and M. Sauer, Antibunching in the Emission of a Single Tetrachromophoric Dendritic System, *J. Am. Chem. Soc.*, 2002, **124**, 14310–14311.
- 14 K. D. Weston, M. Dyck, P. Tinnefeld, C. Müller, D. P. Herten and M. Sauer, Measuring the Number of Independent Emitters in Single-Molecule Fluorescence Images and Trajectories Using Coincident Photons, *Anal. Chem.*, 2002, **74**, 5342–5349.
- 15 J. Sýkora, K. Kaiser, I. Gregor, W. Bönick, G. Schmalzing and J. Enderlein, Exploring fluorescence antibunching in solution for determining the stoichiometry of molecular complexes, *Anal. Chem.*, 2007, **79**, 4040–4049.
- 16 B. J. Berne and R. Pecora, *Dynamic Light Scattering*, Dover, Mineola/New York, 2000.
- 17 R. Feynman, *Feynman's lectures on physics*, Addison-Wesley, Reading, MA, USA, 1964, chapter 18. 4.
- 18 W. J. Thompson, *Angular momentum*, John Wiley & Sons, New York, NY, USA, 1994.
- 19 H. F. Jones, *Groups, representations and physics*, IOP Publishing, Bristol and Philadelphia, 1998, chapter 4.

- 20 P. M. Morse and H. Feshbach, *Methods of Theoretical Physics*, McGraw-Hill, New York, 1953, chapter 7.
- 21 D. Zwillinger, *Handbook of differential equations*, Academic Press, San Diego, CA, USA, 3rd edition, 1990, chapter 96.
- 22 J. Enderlein, I. Gregor, D. Patra, T. Dertinger and B. Kaupp, Performance of fluorescence correlation spectroscopy for measuring diffusion and concentration, *ChemPhysChem*, 2005, **6**, 2324–36.
- 23 M. Abramowitz and I. A. Stegun, *Handbook of Mathematical Functions*, Dover, New York, 1965.
- 24 K. Bahlmann and S. W. Hell, Electric field depolarization in high aperture focusing with emphasis on annular apertures, *J. Microsc.*, 2000, **200**, 59–67.
- 25 K. Bahlmann and S. W. Hell, Depolarization by high aperture focusing, *Appl. Phys. Lett.*, 2000, **77**, 612–614.
- 26 F. Perrin, Mouvement brownien d'un ellipsoïde (I). Dispersion diélectrique pour des molécules ellipsoïdales, *J. Phys. Radium Ser. VII*, 1934, **5**, 497–511.
- 27 F. Perrin, Mouvement brownien d'un ellipsoïde (II). Rotation libre et dépolariation des fluorescences. Translation et diffusion de molécules ellipsoïdales, *J. Phys. Radium Ser. VII*, 1936, **7**, 1–11.
- 28 S. H. Koenig, Brownian Motion of an Ellipsoid. A Correction to Perrin's Results, *Biopolymers*, 1975, **14**, 2421–2423.
- 29 B. K. Müller, E. Zaychikov, C. Bräuchle and D. Lamb, Cross Talk Free Fluorescence Cross Correlation Spectroscopy in Live Cells, *Biophys. J.*, 2005, **89**, 3508–3522.
- 30 M. Wahl, I. Gregor, M. Patting and J. Enderlein, Fast calculation of fluorescence correlation data with asynchronous time-correlated single-photon counting, *Opt. Express*, 2003, **11**, 3583–3591.
- 31 F. L. G. Flecha and V. Levi, Determination of the Molecular Size of BSA by Fluorescence Anisotropy, *Biochem. Mol. Biol. Educ.*, 2003, **31**, 319–322.
- 32 Z. Murtaza, P. Herman and J. R. Lakowicz, Synthesis and spectral characterization of a long-lifetime osmium (II) metal-ligand complex: a conjugatable red dye for applications in biophysics, *Biophys. Chem.*, 1999, **80**, 143–151.
- 33 M. L. Ferrer, R. Duchowicz, B. Carrasco, J. G. de la Torre and A. U. Acuña, The Conformation of Serum Albumin in Solution: A Combined Phosphorescence Depolarization-Hydrodynamic Modeling Study, *Biophys. J.*, 2001, **80**, 2422–2430.
- 34 T. Croguennec, A. Renault, S. Beaufils, J. Dubois and S. Pezennec, Interfacial properties of heat-treated ovalbumin, *J. Colloid Interface Sci.*, 2007, **315**(2), 627–36.
- 35 J. Garcia de la Torre, B. Carrasco and S. E. Harding, Calculation of hydrodynamic properties of globular proteins from their atomic level structure, *Biophys. J.*, 2000, **78**, 719–30.